Spectral broadening of femtosecond pulses into continuum radiation in microstructured fibers

G. Genty, M. Lehtonen, and H. Ludvigsen
Fiber-Optics Group, Metrology Research Institute, Helsinki University of Technology, P.O.Box 3000, FIN-02015 HUT, Finland
Email goery.genty@hut.fi

J. Broeng
Crystal Fibre A/S, Blokken 84, DK-3460 Birkerød, Denmark

M. Kaivola
Department of Engineering Physics and Mathematics, Helsinki University of Technology, P.O.Box 2200, FIN-02015 HUT, Finland

Abstract: We report on the influence of the choice of the pump wavelength relative to the zero-dispersion wavelength for continuum generation in microstructured fibers. Different nonlinear mechanisms are observed depending on whether the pump is located in the normal or anomalous dispersion region. Raman scattering and the wavelength dependence of the group delay of the fiber are found to play an important role in the process. We give an experimental and numerical analysis of the observed phenomena and find a good agreement between the two.

OCIS codes: (190.4370) Nonlinear Optics, Fiber; (190.5650) Raman effect; (190.4380) Four-wave mixing; (230.3990) Microstructure devices; (190.5530) Pulse propagation and soliton.

References and links

1. S. A. Diddams, D. J. Jones, J. Ye, S. T. Cundiff, J. L. Hall, J. K. Ranka, R. S. Windeler, R. Holzwarth, T. Udem, and T. W. Hänsch, "Direct link between microwave and optical frequencies with a 300 THz femtosecond laser comb," Phys. Rev. Lett. **84**, 5102-5105 (2000).
2. T. Udem, R. Holzwarth, and T. W. Hänsch, "Optical frequency metrology," Nature **416**, 233-237 (2002).
3. H. Takara, T. Ohara, K. Mori, K. Sato, E. Yamada, Y. Inoue, T. Shibata, M. Abe, T. Morioka, and K-I. Sato, "More than 1000 channels optical frequency chain generation from single supercontinuum source with 12.5 GHz channel spacing," Electron. Lett. **36**, 2089-2090 (2000).
4. T. M. Monro, W. Belardi, K. Furusawa, J. C. Baggett, N. G. Broderick, and D. J. Richardson, "Sensing with microstructured optical fibres," Meas. Sci. Technol. **12**, 854-858 (2001).
5. T.A. Birks, J. C. Knight, and P. St. J. Russell, "Endlessly single-mode photonic crystal fiber," Opt. Lett. **13**, 961-963 (1997).
6. J. K. Ranka, R. S. Windeler, and A. J. Stentz., "Visible continuum generation in air-silica microstructure optical fibers with anomalous dispersion at 800 nm," Opt. Lett. **25**, 25-27 (2000).
7. S. Coen, A. H. Lun Chau, R. Leonhardt, J. D. Harvey, J. C. Knight, W. J. Wadsworth, and P. St. J. Russell, "White-light supercontinuum generation with 60-ps pump pulses in a photonic crystal fiber," Opt. Lett. **26**, 1356-1358 (2001).
8. P. A. Champert, S. V. Popov, and J. R. Taylor, "Generation of multiwatt, broadband continua in holey fibers," Opt. Lett. **27**, 122-124 (2002).
9. A. V. Husakou and J. Herrmann, "Supercontinuum generation of higher–order solitons by fission in photonic crystal fibers," Phys. Rev. Lett. **87**, 203901 (2001).
10. J. Herrmann, U. Griebner, N. Zhavoronkov, A. V. Husakou, D. Nickel, J. C. Knight, W. J. Wadsworth, P. St. J. Russell, and G. Korn, "Experimental evidence for supercontinuum generation by fission of higher-order solitons in photonic fibers," Phys. Rev. Lett. **88**, 173901 (2002).
11. J. M. Dudley, L. Provino, N. Grossard, H. Maillotte, R. S. Windeler, B. J. Eggleton, and S. Coen, "Supercontinuum generation in air-silica microstructured fibers with nanosecond and femtosecond pulse pumping," J. Opt. Soc. Am. B **19**, 765-771 (2002).
12. B. R. Washburn, S. E. Ralph, and R. S. Windeler, "Ultrashort pulse propagation in air-silica microstructure fiber," Opt. Exp **10**, 575-580 (2002).
13. G. P. Agrawal, *Nonlinear Fiber Optics* (Academic Press, New York, 2001).
14. K. J. Blow and D. Wood, "Theoretical description of transient stimulated Raman scattering in optical fibers," IEEE J. Quantum Electron. **25**, 2665-2673 (1989).

#1605 - $15.00 US Received August 21, 2002; Revised September 25, 2002

15. N. Akhemediev and M. Karlsson, "Cherenkov radiation emitted by solitons in optical fibers," Phys. Rev. A **51**, 2602-2607 (1995).
16. Y. Kodama and A. Hasegawa, "Nonlinear pulse propagation in monomode dielectric guide," IEEE J. Quantum Electron. **23**, 510-524 (1987).
17. F. M. Mitschke and L. F. Mollenauer, "Discovery of the soliton self-frequency shift," Opt. Lett. **11**, 659-661 (1986).
18. P. Beaud, W. Hodel, B. Zysset, and H. P. Weber, "Ultrashort pulse propagation, pulse breakup, and fundamental soliton formation in a single-mode optical fiber," IEEE J. Quantum Electron. **23**, 1938-1946 (1987).
19. J. P. Gordon, "Theory of the soliton self-frequency shift," Opt. Lett. **11**, 662-664 (1986).
20. Data kindly provided by R. H. Stolen.
21. N. Nishizawa and T. Goto, "Experimental analysis of ultrashort pulse propagation in optical fibers around zero-dispersion region using cross-correlation frequency resolved optical gating," Opt. Exp. **8**, 328-334 (2001).
22. V. P. Yanovsky and F. W. Wise, "Nonlinear propagation of high-power, sub-100-fs pulses near the zero-dispersion wavelength of an optical fiber," Opt. Lett. **19**, 1547-1549 (1994).
23. J. E. Rothenberg and D. Grischkowsky, "Observation of the formation of an optical intensity shock and wave breaking in the nonlinear propagation of pulses in optical fibers," Phys. Rev. Lett. **62**, 531-534 (1989).

1. Introduction

Microstructured fibers (MFs) show great potential for various applications in the fields of optical frequency metrology, sensor technology, and optical telecommunications [1-4]. These fibers consist of a solid silica core surrounded by an array of air holes running along the fiber. The structure provides a wavelength-dependent effective index for the cladding and can allow single-mode guidance throughout the visible and near infrared [5]. By varying the arrangement and size of the holes, the dispersion properties of the fiber can be tailored in broad ranges and, for instance, the effective area of the propagating mode can be adjusted to enhance the optical nonlinearities in the fiber. The combination of the unique dispersion properties and enhanced nonlinearities can be used for advantage to obtain efficient generation of supercontinuum (SC) radiation when the fiber is pumped with short pulses of laser light with wavelength located in the vicinity of the zero-dispersion wavelength (ZDW) [6-8]. Attempts have been made to identify the different nonlinear contributions in the formation of the continuum [9-12]. In this paper, we present experimental results on the influence of the relative detuning between the ZDW of the MF and the wavelength of the pump pulses on the SC generation. Along with the experimental observations, we present a numerical analysis of the observed phenomena that gives insight into the physical mechanisms responsible for the SC formation in microstructured fibers. We conclude that when the pump wavelength lies in the anomalous dispersion region, it is the soliton decay due to Raman scattering that initiates the formation of the continuum. We have experimentally observed that this mechanism can allow a broad continuum to be generated even if the pump wavelength is detuned by as much as 200 nm from the ZDW. In the normal dispersion regime, self-phase modulation is the process that initiates the continuum generation. The combination of four-wave mixing and Raman processes then extends the width of the continuum further.

2. Experimental setup

The experimental setup is depicted in Fig. 1. The output pulse train of a mode-locked Ti:Sapphire laser (Tsunami/SpectraPhysics) is coupled into a MF (Crystal Fibre A/S) using an aspheric lens with a focal length of 4.5 mm and a numerical aperture of 0.55. The laser produces 100 fs pulses (FWHM) at a repetition rate of 80 MHz and with an average power of up to 1.7 W. An afocal system is placed before the coupling lens in order to expand the diameter of the laser beam from 1 to 5 mm. A 30-dB isolator prevents reflections back into the laser. With this system, the coupling efficiency is estimated to be around 20-30 % depending on the core diameter of the MF. The optical spectrum is recorded at the fiber output using an

#1605 - $15.00 US Received August 21, 2002; Revised September 25, 2002

optical spectrum analyzer (Ando AQ6315). The average laser output power is measured with a calibrated calorimeter.

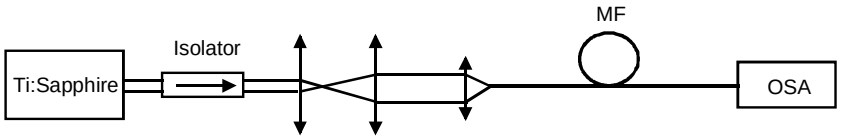

Fig. 1. Experimental setup. MF: Microstructured fiber, OSA: Optical spectrum analyzer.

3. Pumping in the anomalous dispersion region

First the generation of the continuum was studied in a 5 m long piece of highly birefringent MF with an elliptical core of dimensions 1.5 μm × 2.4 μm. A microscope image of the fiber cross-section is shown in the inset of Fig. 2. In theory, the fiber can allows for the propagation of up to three different modes in the visible but in practice we could only excite the fundamental mode for wavelengths from 400 nm to beyond 1500 nm. No higher-order modes was observed during any of the experiments reported here. The group delay (GD) and dispersion (D) of the MF are given in Fig. 2 as functions of wavelength. The ZDW of the fiber is located at around 650 nm for the slow axis. The beat length of the two orthogonal polarization modes in the fiber is estimated to be less than 0.2 mm at 800 nm.

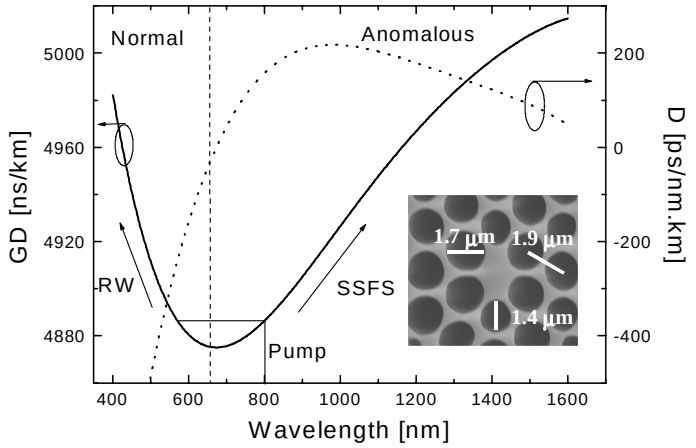

Fig. 2. Group delay and dispersion of the highly birefringent MF. RW: radiated waves, SSFS: soliton self-frequency shift. The inset shows a microscope image of the fiber cross-section together with the relevant dimensions.

The direction of the linear polarization of the pump pulses was chosen to be parallel to the slow polarization axis of the MF. In that case, all the spectral components were found to maintain their polarization along the propagation. The output spectra recorded for increasing pump power with the pump wavelength λ_p tuned to 804 nm are presented in Fig. 3. The initial pulse first decays into several sub-pulses, which appear in the optical spectra as distinct red-shifted Stokes components. Blue-shifted anti-Stokes components are simultaneously generated and a gap is formed in the vicinity of the ZDW. Increasing the pump power further leads to a merging of the various spectral components, and to a subsequent formation of a supercontinuum that extends from 400 to beyond 1400 nm.

#1605 - $15.00 US Received August 21, 2002; Revised September 25, 2002

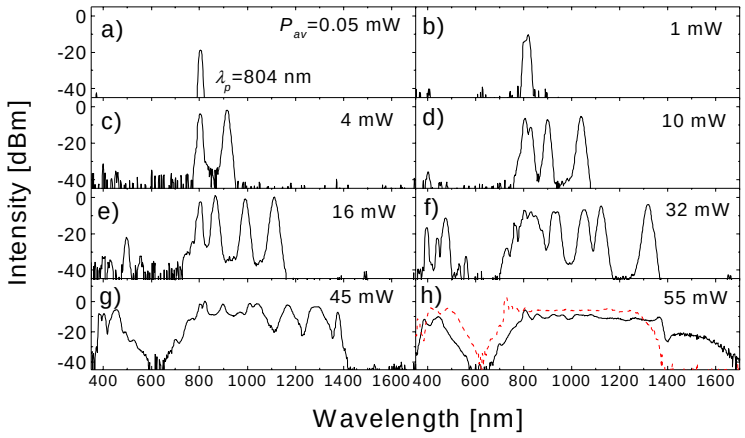

Fig. 3. Evolution of the input pulse into supercontinuum in the highly birefringent MF.

To understand the underlying mechanisms leading to the supercontinuum generation, we have solved the nonlinear Schrödinger equation (NSE) using a standard split-step Fourier algorithm. In a frame of reference moving at the group velocity of the pulse, the NSE can be written as [13]

$$\frac{\partial A}{\partial z}+\frac{\alpha}{2}-\sum_n \frac{i^{n+1}}{n!}\beta_n \frac{\partial^n A}{\partial T^n}= i\gamma(1+\frac{i}{\omega_0}\frac{\partial}{\partial T})A\int_{-\infty}^{+\infty} R(T')\left|A(z,T-T')\right|^2 dT', \quad (1)$$

where A is the slowly varying envelope of the electric field and the coefficients α, β_n and γ represent the losses, the nth order of the Taylor series expansion of the propagation constant around the carrier frequency ω_0, and the nonlinear coefficient, respectively. The values of these parameters at 800 nm for the highly birefringent fiber are given in Table 1.

Table 1. Parameters for the highly birefringent MF (λ = 800 nm).

β_2 (ps^2/km)	β_3 (ps^3/km)	β_4 (ps^4/ km)	β_5 (ps^5/ km)	β_6 (ps^6/km)	γ (/W/km)
-57.5	1.35×10^{-1}	3.12×10^{-6}	-2.90×10^{-7}	3.69×10^{-10}	~100

The convolution operation on the right-hand side of Eq. (1) accounts for both the instantaneous and delayed nonlinear response of the propagation medium. The derivative term on the right-hand side of Eq. (1) represents the self-steepening (SS) effect. We retain terms up to the 6th order in the Taylor series expansion of the propagation constant, which ensures the accuracy of the calculations over a bandwidth of several hundreds of nanometers [14]. For the nonlinear response of the fiber we use the expression [13]

$$R(T)=(1-f_R)\delta(T)+f_R h_R(T), \quad (2)$$

where f_r=0.18 [13] represents the fractional contribution of the Raman delayed response $h_R(T)$, which is approximated by

$$h_R(T)=\frac{\tau_1^2+\tau_2^2}{\tau_1\tau_2^2}e^{-\frac{T}{\tau_2}}\sin\left(\frac{T}{\tau_1}\right), \quad (3)$$

#1605 - $15.00 US
Received August 21, 2002; Revised September 25, 2002

with τ_1 and τ_2 taken to be 12.2 fs and 32 fs, respectively [13]. Equation (1) describes accurately the pulse propagation along optical fibers for pulses as short as 50 fs [13]. We apply the model to simulate the first stages of the continuum formation, i.e., as long as the bandwidth does not exceed 500 nm at the output of the fiber. To assess the role that Raman scattering (RS) plays in the generation of SC, we solve Eq. (1) with (Fig. 4c-d) and without (Fig. 4a-b) the Raman term included, using the parameter values of our MF and assuming a Gaussian shape for the input pulse. The contribution of the higher-order dispersive terms (HOD), i.e., terms proportional to β_n in Eq. (1) with $n \geq 3$, was also investigated (Fig. 4b-d). When neither the higher-order dispersive terms nor the Raman scattering contribution are included, as is the case in Fig. 4a, the spectrum evolves periodically along the fiber as that of a higher-order soliton. When including the HOD terms (Fig. 4b), the initial pulse starts to decay into several sub-pulses causing the central part of the spectrum to be broadened. The most noteworthy feature is the appearance of the blue anti-Stokes components in the spectrum. These components arise from the perturbation by HOD of the different sub-pulses propagating along the fiber. Indeed, the sub-pulses shed away energy in order for the pulse to be able to propagate as a fundamental soliton, and this radiated energy is found in the spectrum as anti-Stokes lines [15]. These anti-Stokes components carry a substantial part of the total energy whereas the red side of the spectrum is found to expand rather moderately. Adding the Raman term in the NSE produces results in much better agreement with our experimental observations (see Fig. 4c-d and Fig. 3c-e), particularly as regards to the strong spreading of the pulse spectrum towards the near infrared and the appearance of the distinct Stokes peaks. This result differs from the recent predictions given in Ref. 9 where Raman scattering is assumed to be negligible and, consequently, the extension of the continuum to the infrared is not significant. Our analysis shows, however, the RS cannot be neglected when modeling and interpreting supercontinuum generation with femtosecond pump pulses in MFs. The initially slow growth of the blue anti-Stokes components is also in agreement with the experiments.

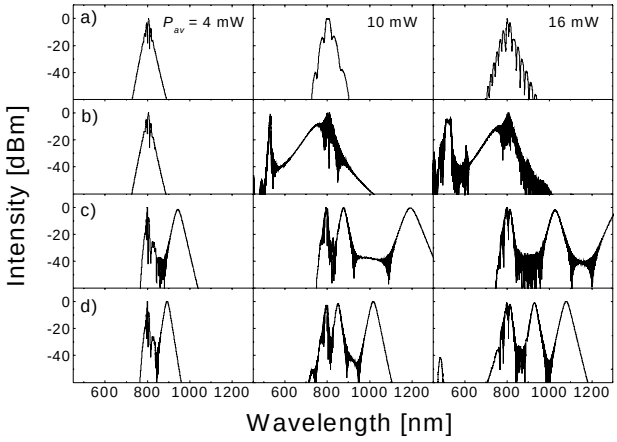

Fig. 4. Simulation of the first stages of the continuum formation. a) only β_2, b) β_2 + SS + HOD, c) β_2 + RS + SS and d) β_2 + HOD + RS + SS.

The onset of the continuum formation can be explained as follows. The pulse is initially compressed due to the combined effect of nonlinearities and anomalous dispersion before it breaks into multiple solitons. For a pulse width of $T_{FWHM} \approx 100$ fs, the dispersion length of the fiber is equal to $L_D=T_0^2/|\beta_2| \approx 6.5$ cm at 804 nm with T_0 being related to T_{FWHM} by $T_0=T_{FWHM}/1.665$ assuming a Gaussian pulse shape. Consequently, for a pulse peak power exceeding P_p=230 W (P_{av}=2 mW) the nonlinear length $L_{NL}=1/(\gamma P_p)$ is shorter than L_D and the pulse launched into the fiber corresponds to an Nth-order bound-state soliton. Such a soliton is constituted of N fundamental solitons (N is the nearest integer for

#1605 - $15.00 US Received August 21, 2002; Revised September 25, 2002

$\sqrt{L_D/L_{NL}} = T_0\sqrt{\gamma P_p/|\beta_2|}$) whose relative group velocities and amplitudes are given by the real and imaginary parts of the eigenvalues obtained by solving the simplified NSE using the inverse scattering method [16]. The amplitudes and widths of the individual constituents can be expressed as [16]

$$A_k = \frac{A_0(2A_0 - 2k + 1)}{N}, \tag{4}$$

$$T_k = \frac{T_0}{2A_0 - 2k + 1}, \tag{5}$$

with k∈[1,*N*] and A_0 being equal to $\sqrt{P_p}$. In the absence of perturbations, i.e., when the HOD and RS terms are neglected, the real parts of the eigenvalues are degenerate and the *N*th-order soliton is a bound-state that propagates with periodical changes in its spectrum. This is the case in Fig. 4a. The HOD and RS terms tend to break the degeneracy of the eigenvalues making the different constituents travel with different group velocities. Therefore, the bound-state of the *N*th-order soliton is broken and the initial pulse decays into several sub-pulses which propagate independently as fundamental solitons. Even though HOD can lead to soliton decay by itself, we found that the threshold is lower for RS than for HOD to induce the decay in the case of femtosecond pulses and our MF. In other words, the soliton decay is primarily due to Raman scattering. The number of solitons that appear in the spectrum is equal to the soliton order *N* of the pulse launched into the fiber, provided the fiber is long enough. The fiber lengths required to observe the *N* individual constituents increases with *N* and can exceed, for large *N* values, tens of times the soliton period z_0 defined as $\pi L_D/2$. This is because the constituent solitons are stripped off one by one from the initial bound-state. They all undergo soliton self-frequency shift (SSFS) [17] and, therefore, appear in the spectrum as distinct red-shifted components. The solitons are perturbed by HOD while propagating into the MF and, as a consequence, radiate energy in order to maintain their shape. This radiated energy appears in the spectrum as anti-Stokes peaks. They are generated with a much lower intensity than the Stokes lines that correspond to the solitons [18], as is evident in Figs. 3d and 4d. Both the Stokes and anti-Stokes lines gradually shift further into the red and blue, respectively, as the input power is increased. In our experiments, the anti-Stokes peaks became visible in the spectra only when the input power exceeded 10 mW. Below this level, we could not distinguish them from the noise of the spectrum analyzer.

A simple model shows that the frequency shift $\Delta\nu_k$ that a fundamental soliton of width T_k has undergone after propagating a distance *z* along the MF is inversely proportional to T_k^4 [19]:

$$\Delta\nu_k = \frac{1.2904\lambda^2 D(\lambda) q(T_k) z}{T_k^{\,4}}, \tag{6}$$

where $D(\lambda)$ represents the dispersion and $q(T_k)$ is the value of the overlap integral of the pulse and the Raman gain spectra. Since the *N* fundamental solitons have originally different amplitudes and widths, as can be seen from Eqs. (4) and (5), the center frequencies of the different solitons undergo different shifts to the infrared. Therefore they appear as distinct Stokes components in the optical spectrum. This is in good agreement with our experimental observations. Indeed, in Fig. 3e $\sqrt{L_D / L_{NL}}$ is equal to 3.9 and we observe 4 peaks in the spectrum. In Fig. 3f, $\sqrt{L_D / L_{NL}}$ = 5.8 and the number of distinct peaks in the spectrum is

#1605 - $15.00 US Received August 21, 2002; Revised September 25, 2002

six. Note that in this case, the fiber length is more than 40 times longer than the soliton period, which is why the *N* Stokes components are observed. To emphasize the role played by Raman scattering in the process, we have measured experimentally the center wavelength of the first Stokes component appearing in the spectrum and followed its subsequent shift when increasing the input power. The measurements were performed for two different fiber lengths: 20 cm and 5 m, which approximately correspond to $2z_0$ and $40z_0$, respectively. The results are indicated as squares in Fig. 5.

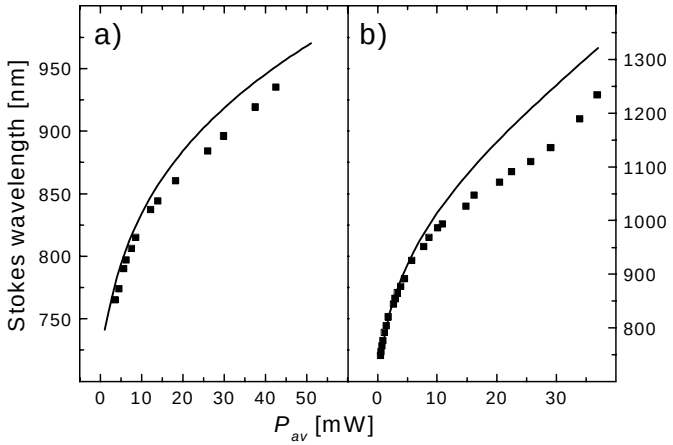

Fig. 5. Wavelength of the first Stokes component appearing in the spectrum vs. average input power for *z* equal to a) 20 cm and b) 5 m. The squares and the solid line represent the measured and calculated shift, respectively.

Using Eqs. (5) and (6) the theoretical shift was calculated as a function of the average input power. In the model, the full experimental data of the Raman gain in a standard optical fiber were implemented [20]. The theoretical results are plotted as solid lines in Fig. 5. A reasonable agreement with the measured values is found. In particular, the wavelength shift is an increasing function of the input power and for equal input powers the shift is greater for the longer piece of fiber. We observed that the number of the Stokes components was limited to three in the case of the 20 cm long fiber, whereas up to six Stokes peaks were observed for the longer fiber. This reflects the fact that the fiber length is only twice the soliton period for the 20 cm piece of fiber. The inclusion of the self-steepening term is essential to correctly reproduce the experimental measurements. The difference between the simulation and experiment becomes larger as the input power increases. Two factors could explain this difference. First, the model does not take into account the energy radiated by the solitons in the form of anti-Stokes lines. Including this should cause the soliton amplitude, and therefore also the frequency shift, to be decreased as the soliton propagates down the fiber. Secondly, the original values of the amplitude and width of the different constituents in Eq. (3) are slightly affected by RS. Taking this into account would also reduce the frequency shifts.

Figure 6 illustrates the SC formed by using the 20 cm and 5 m long MF for the same input pulse parameters (λ_p=737 nm, P_{av}=40 mW). Due to SSFS, the center wavelengths of the various solitons have shifted further to the red in the longer fiber, resulting in an extended continuum compared to the shorter MF.

#1605 - $15.00 US Received August 21, 2002; Revised September 25, 2002

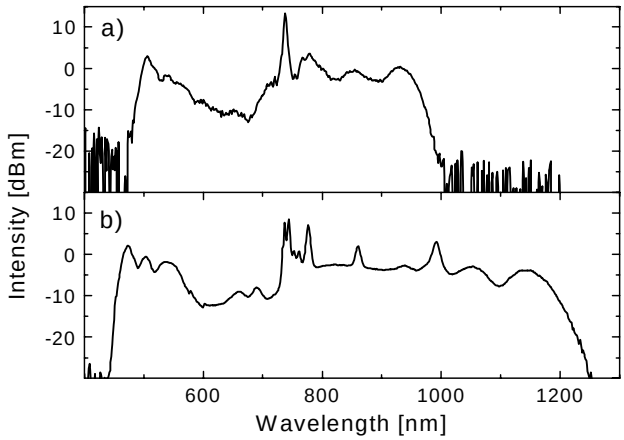

Fig. 6. Supercontinuum generated in a) 20 cm and b) 5 m long MF.

We also simulated the temporal evolution of the output by solving Eq. (1) using the parameter values of our fiber. The time trace includes several delayed pulse components as is illustrated in Fig. 7. The separated delayed pulses correspond to the red-shifted Raman solitons. They have a soliton-type profile (plotted as an inset in Fig. 7), which indicates that the delayed pulses have a fundamental soliton nature.

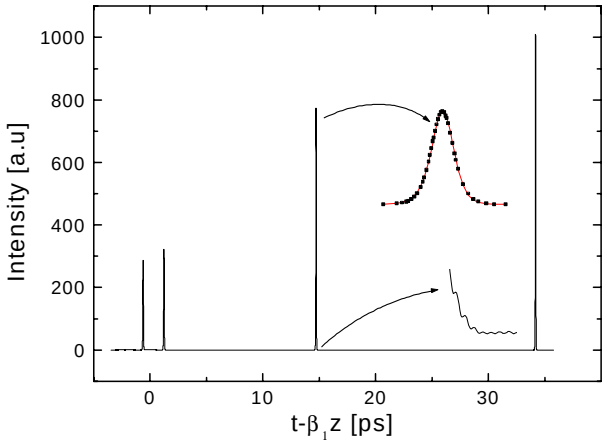

Fig. 7. Simulated time trace of the output. Both the sech fit and the modulation on the soliton tails resulting from interference between the solitons and the dispersive waves are outlined.

The delays experienced by the multiple solitons with respect to the remains of the pump pulse propagating in the fiber increase with the peak power and thus with the frequency shift. This is due to a decrease of the group velocity as the solitons shift towards the infrared. As expected, the multiple solitons have different amplitudes with the soliton experiencing the largest delay exhibiting the largest amplitude. Furthermore, we notice that dispersive waves are superimposed onto the temporal profile of the delayed solitons. Using spectral filtering in the simulations, we could identify these waves with the anti-Stokes components of the spectrum. This indicates that the Stokes and anti-Stokes components initially travel at the same group velocity so that energy transfer from the solitons to the radiated waves is possible. This phenomenon was recently confirmed by experiments in dispersion-decreasing fibers [21]. The fact that the Stokes and anti-Stokes frequency components travel at the same speed

#1605 - $15.00 US Received August 21, 2002; Revised September 25, 2002

allows one to explain the gap observed in the spectrum of the continuum when the pump is located in the anomalous dispersion region. The Stokes lines are generated on the red side of the pump up to 1400 nm, which implies that the anti-Stokes lines should be found between 550 and 400 nm, as is indicated by the arrows in Fig. 2. This is indeed the case in our experiments, as can be observed in Fig. 3. Therefore, pumping far from the ZDW on the anomalous side allows one to increase the bandwidth of the supercontinuum, but at the expense of widening the gap between the Stokes and anti-Stokes peaks. For comparison, the spectrum of the SC generated with λ_p=722 nm and P_{av}=55 mW is plotted as a dashed line in Fig. 3h. For clarity, an arbitrary vertical offset has been added. The width of the gap and bandwidth of the SC are reduced as could be predicted from the group-delay profile of the fiber.

In our experiments, we were able to generate a broad supercontinuum with the pump wavelength tuned to as far as 200 nm from the ZDW. The tuning range of our laser did not allow us to move the pump wavelength further. Furthermore, the continuum could not be extended beyond 1400 nm except for an unstable extra feature that we attribute to spontaneous Raman scattering. This limitation for the extension of the SC to the red stems from the strong OH absorption peak of the fiber. The peak is located at around 1400 nm and its magnitude exceeds 1 dB/m. For a 5 m long fiber, the limitation was observed independently of the pump wavelength. Removing this absorption peak in the manufacturing process should allow increasing the width of the continuum. We also point out that, according to our simulations, the frequency shift of the solitons is enhanced for smaller values of third-order dispersion, thus leading to a formation of a wider continuum.

Next we consider the effects of degenerate four-wave mixing (FWM) to the continuum formation, i.e., a process where two pump photons generate a Stokes and an anti-Stokes photon:

$$2\omega_p \rightarrow \omega_s + \omega_{as}. \tag{7}$$

Here ω_p, ω_s and ω_{as} correspond to the pump, Stokes, and anti-Stokes frequencies, respectively. Being a coherent process, four-wave mixing is efficient only, if the phase-matching condition is fulfilled [13], i.e.,

$$\Delta\phi = \phi(\omega_a) + \phi(\omega_{as}) - 2\phi(\omega_p) = L\left(2\sum_n \frac{\beta_{2n}}{(2n)!}(\omega_a - \omega_p)^{2n} + 2\gamma P_p\right) = 0. \tag{8}$$

Here β_{2n} is the $2n$th derivative of the propagation constant β with respect to the frequency, P_p the peak power of the pump pulse and L is the fiber length. Note that only the even terms of the series expansion of β contribute to the phase-matching condition. Using the parameter values of the elliptical-core MF and retaining only terms up to the fourth order, the Stokes and anti-Stokes wavelengths as due to FWM are shown in Fig. 8 as a function of the pump wavelength. The results are plotted for three input peak powers. For a pump wavelength located in the anomalous dispersion region, the phase-matching condition is mainly governed by the induced nonlinear phase shift (term $2\gamma P_p$ in Eq. (8)). As a consequence, the generated Stokes and anti-Stokes wavelengths are quasi-linear functions of the pump wavelength and lie in value close to that.

#1605 - $15.00 US Received August 21, 2002; Revised September 25, 2002

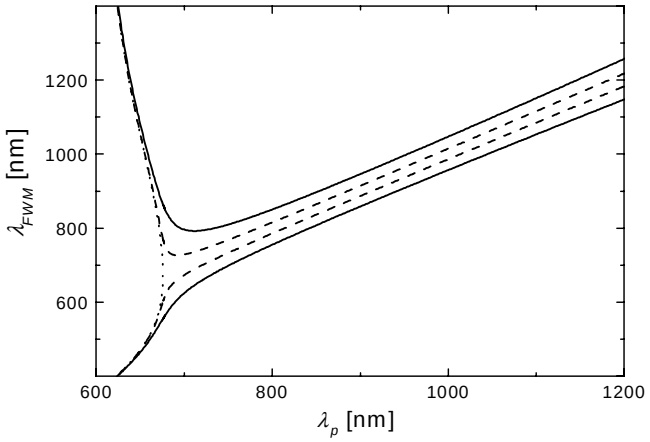

Fig. 8. Phase-matching diagram calculated for the elliptical-core MF. The dotted, dashed, and solid lines represent the phase-matching condition for a peak power of ~0, 0.5 and 5 kW, respectively.

The multiple solitons generated through Raman scattering can act as pump waves for the mixing process. The corresponding Stokes and anti-Stokes wavelengths are generated in the vicinity of the spectral bands of the solitons, thus contributing to their merging.

The blue-shifted frequencies resulting from the field radiated by the solitons can theoretically also serve as pumps in FWM. However, the large frequency shifts associated with the Stokes and anti-Stokes components make the process very weak. FWM can also occur between the radiated waves and the Raman solitons. The generated wavelengths fall in the gap observed in the measured spectra. The fact that these components are not present in the spectra indicates that the mixing process is weak. This can again be explained as being due to the large frequency difference between the solitons and the radiated waves. If the fiber is shortened to 1 m, the gap between the red and blue parts of the spectrum becomes filled indicating that in this case FWM is more efficient. Pumping closer to the ZDW also considerably reduces the depth of the gap. This is because the amount of dispersion is now substantially smaller and the initial broadening of the spectrum due to SPM will allow generation of frequencies closer to the ZDW. The phase-matching condition is then easily fulfilled and the gap around the ZDW will be filled. Figure 9 shows the continuum generated in a 1 m long fiber with λ_p=731 nm. The combination of the short length of fiber and proximity of λ_p to the ZDW allows for efficient FWM, which fills the gap between the blue and red spectral components. The result is an almost flat continuum from 400 nm to 1400 nm.

#1605 - $15.00 US Received August 21, 2002; Revised September 25, 2002

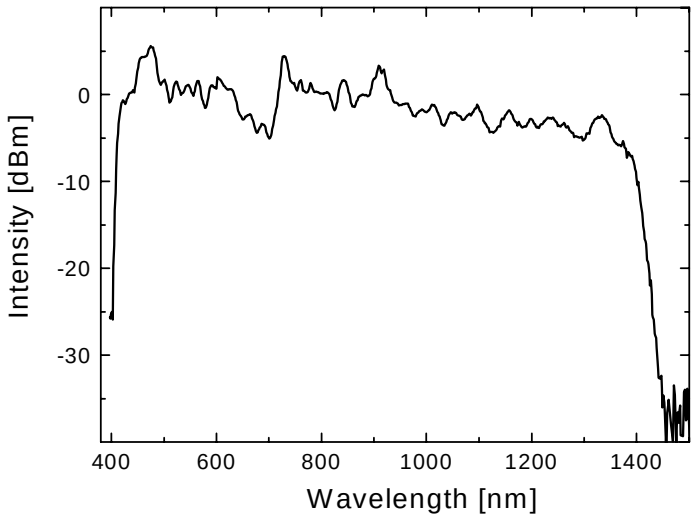

Fig. 9. Supercontinuum generated in 1 m of the highly birefringent MF. P_{av}=84 mW and λ_p=731 nm.

Finally, we simulated the spectrogram of the continuum as it propagates down the MF. The result is shown in the animation in Fig. 10. This provides a convenient way to observe all the aforementioned mechanisms. In particular, the stripping of Raman solitons off from the pump and the simultaneous emission of the anti-Stokes components is a development to be noticed. The dispersive nature of the anti-Stokes components is confirmed through their fast spreading in time. Four-wave mixing between the Stokes and anti-Stokes components is also observed.

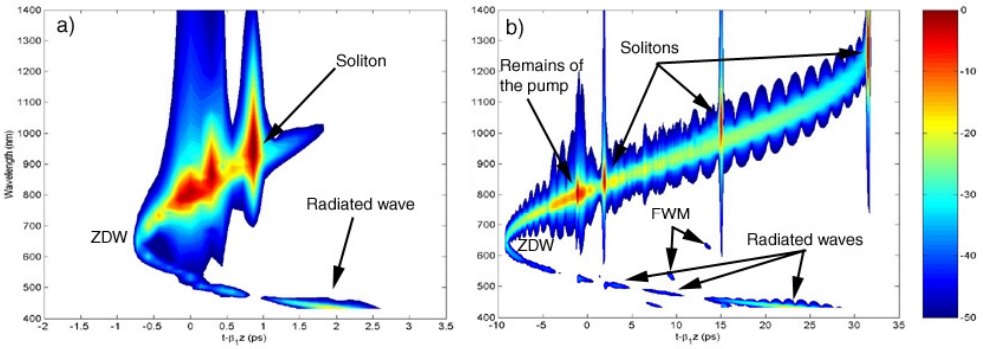

Fig. 10. Simulation of the spectrogram after a) 10 cm and b) 1 m of propagation along the MF. P_{av}=20 mW and λ_p=804 nm. The normalized intensity is plotted in a logarithmic scale. The animation represents the formation of the continuum as the pulses propagate along the fiber, each frame corresponding to a step of 1 cm of propagation.

4. Pumping in the normal dispersion region

Using the same experimental setup as before, the light of the Ti:Sapphire laser was coupled into a 14 meters long MF with a round core of 2.5 μm diameter whose ZDW is located in the vicinity of 950 nm. The pump wavelength was set to lie in the normal dispersion region of the fiber at 746 nm. A microscope image of the fiber cross-section, and the group delay and dispersion of the fiber are presented in Fig. 11. We did not observe any significant

#1605 - $15.00 US
Received August 21, 2002; Revised September 25, 2002

dependence of the generated continuum on the input polarization. This is as expected for a symmetric stucture. As for the previous fiber type, the pulses were found to propagate in the fundamental mode for wavelengths between 600 nm and 1400 nm. The parameters of the fiber at 860 nm are given in Table 2.

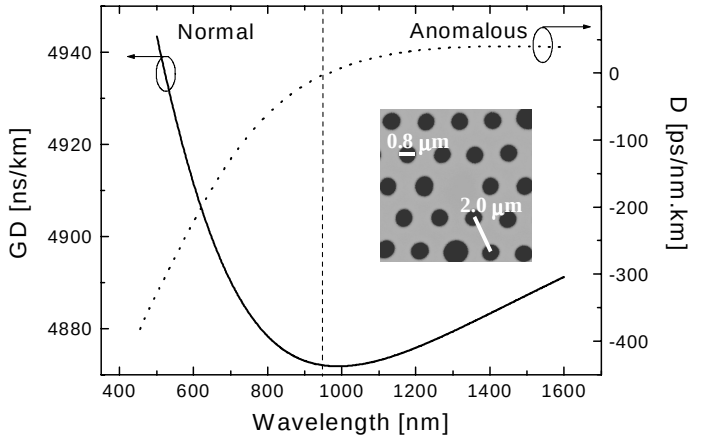

Fig. 11. Group delay and dispersion of the round-core MF. The inset shows a microscope image of the fiber cross-section together with the relevant dimensions.

Table 2. Parameters for the round-core MF (λ = 860 nm).

β_2 (ps^2/km)	β_3 (ps^3/km)	β_4 (ps^4/km)	β_5 (ps^5/km)	β_6 (ps^6/km)	γ (/W/km)
11.5	2.62×10^{-2}	-6.14×10^{-5}	-1.25×10^{-8}	5.04×10^{-11}	~50

Figure 12 illustrates the evolution of the input pulse into a supercontinuum. The main feature to be observed in the output spectra is the fact that the continuum does not extend beyond the ZDW. Bright solitons cannot propagate in the normal dispersion region and the mechanism leading to the formation of the SC relies mainly on self-phase modulation (SPM) and RS.

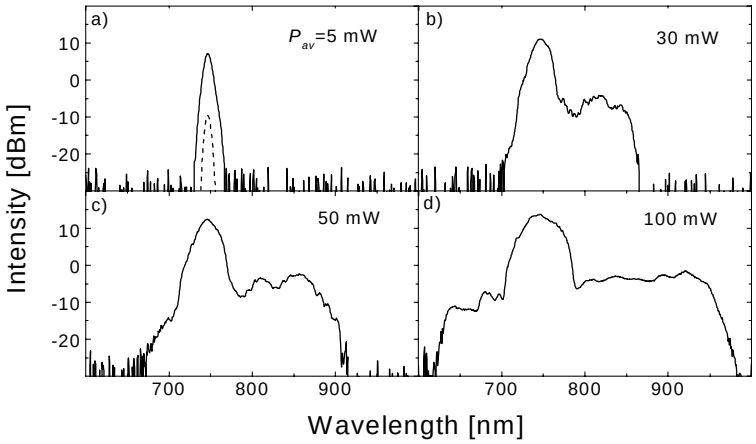

Fig. 12. Evolution of the input pulse into supercontinuum in the 14 m long round-core MF for λ_p=746 nm.

#1605 - $15.00 US
Received August 21, 2002; Revised September 25, 2002

The spectrum of the input pulse first broadens symmetrically due to SPM as seen in Fig. 12a. At low input powers, the rapid broadening of the pulse due to the high value of the dispersion (β_2 =65 ps^2/km) leads to a substantial decrease of the peak power and the SPM-induced broadening is limited to around 100 nm. When increasing the input power, new frequencies are generated on the red side of the spectrum through stimulated Raman scattering, thereby resulting in an asymmetrical broadening as is observed in Fig. 12b-d. For average powers in excess of 50 mW, a tail starts to emerge on the blue side of the spectrum (see Fig. 12c-d). We attribute its origin to the self-steepening effect.

The pump wavelength was subsequently tuned to 831 nm, which is closer to the ZDW, but is still in the normal dispersion region. The spectral evolution is illustrated in Fig. 13.

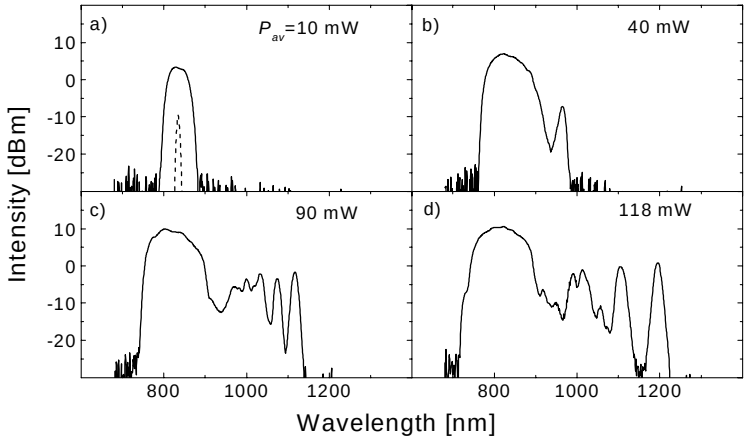

Fig. 13. Evolution of the input pulse into supercontinuum in the 14 m long round-core MF for λ_p=831 nm.

The initial behavior is similar to the case of pumping at 746 nm. Nevertheless, the dispersion value is now smaller, which results in an enhanced SPM-induced broadening of the spectrum (compare Fig. 13a to Fig. 12a). The SPM-induced broadening allows extending the spectrum into the vicinity of the ZDW. The energy present close to the ZDW serves as a seed for efficient four-wave mixing, which extends the continuum further to the red. In particular, we observe a sudden extension of the spectrum to the red when the input power exceeds a certain threshold value, which confirms the significance of FWM in the SC formation [22]. The phase-matching diagram of Fig. 14 shows that FWM is most efficient in the vicinity of the ZDW. This explains the depletion observed in the spectra of Fig. 13c-d at around 950 nm. At this stage, the wave packet located in the anomalous dispersion region forms multiple bound states that rapidly evolve into solitons. These solitons subsequently experience SSFS (see Fig. 13c-d), which expands the continuum further to the infrared. Due to the steep slope of the group-delay profile at the blue wavelengths, most of the anti-Stokes components corresponding to the waves radiated by the solitons lie in between the pump wavelength and the ZDW.

#1605 - $15.00 US Received August 21, 2002; Revised September 25, 2002

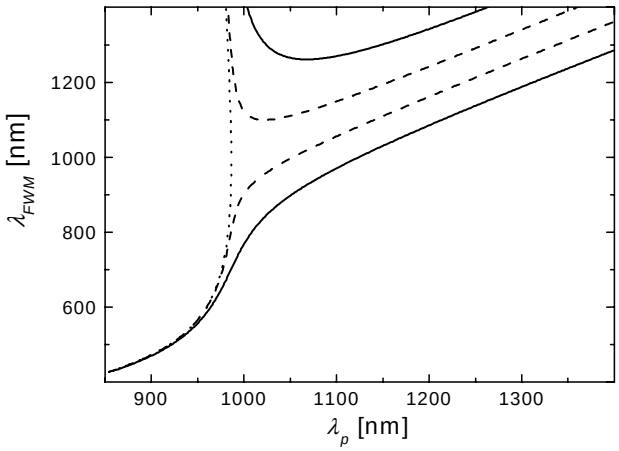

Fig. 14. Phase-matching diagram calculated for the round-core MF. The dotted, dashed, and solid lines represent the phase-matching condition for a peak power of ~0, 0.5 and 5 kW, respectively.

Increasing the pump power results in extending the continuum further to the infrared. Nevertheless, in that case, spectral components beyond 1230 nm were observed to be strongly attenuated. This is due to the long fiber length and the strong OH absorption peak (1 dB/m) located at around 1230 nm. Indeed, since the energy transferred to the red part of the spectrum is now much lower than in the case when pumping in the anomalous dispersion region, the magnitude of this absorption peak is enough to affect the propagation of solitons beyond the absorption wavelength. Spectral components beyond 1230 nm are generated due to SSFS in the first meter of the fiber but they are subsequently strongly attenuated in the spectrum measured after 14 m of propagation (≈ 14dB attenuation).

Shortening the fiber and tuning the pump wavelength closer to the ZDW should permit transferring more energy to the anomalous region through SPM and FWM and the losses experienced by the solitons to be reduced. Therefore, spectral components beyond 1230 nm should more clearly be observed. This was verified experimentally in a 1-m piece of fiber with the results illustrated in Fig. 15a. The limit is now set, as in the case of anomalous dispersion, by the second, stronger absorption peak located at around 1400 nm (>1.5 dB/m). Using the parameter values of the MF, we solved the NSE for propagation of infrared pulses through 1 m of the fiber. The results are presented in Fig. 15b. Reasonable agreement is found between the measured and simulated spectra and, in particular, the simulation affirms the expansion of the continuum beyond the ZDW and the subsequent formation of solitons. The spectral broadening towards the low wavelengths is less pronounced in the simulation and could be due to the uncertainty in the measured dispersion curve at these wavelengths.

#1605 - $15.00 US Received August 21, 2002; Revised September 25, 2002

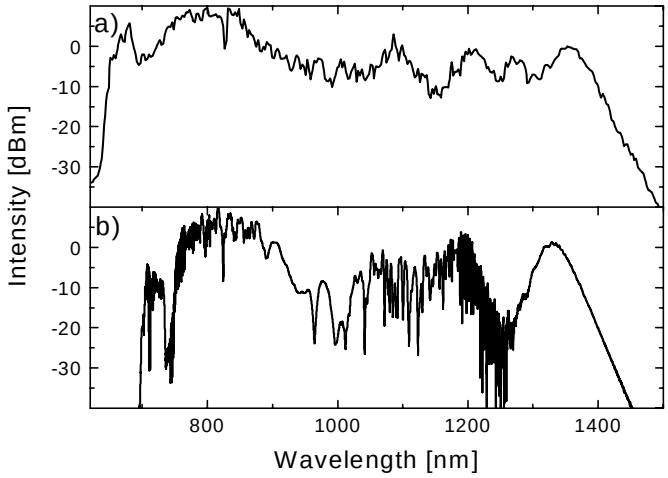

Fig. 15. Supercontinuum generated in 1 m of the round-core MF: a) measured and b) simulated. λ_p=860 nm, P_{av}=120 mW, T_{FWHM}=130 fs.

To verify the role played by SPM in the SC formation, we performed spectral measurements of the continuum formed in the 1 m long MF for different pulse widths keeping the average power of the pump pulse constant. Doing so, the total input energy is preserved, but the input peak power is varied. The results are presented in Fig. 16. For broader pulses, the continuum is confined into the normal dispersion region and its width is limited to 200 nm. As the pulse width is reduced and, consequently, the peak power is increased, the width of the continuum extends further to the blue and to the red, as is typical of SPM broadening. For the shorter pulses, more energy is transferred into the anomalous dispersion region through SPM, which results in an extended continuum due to SSFS. Another interesting phenomenon is the flat spectral feature that extends from 780 to 850 nm. This plateau is a manifestation of optical wave breaking [23]. Its height decreases with the pulse width. This is because optical wave breaking is very sensitive to the ratio L_D / L_{NL}, which decreases when the pulse becomes narrower.

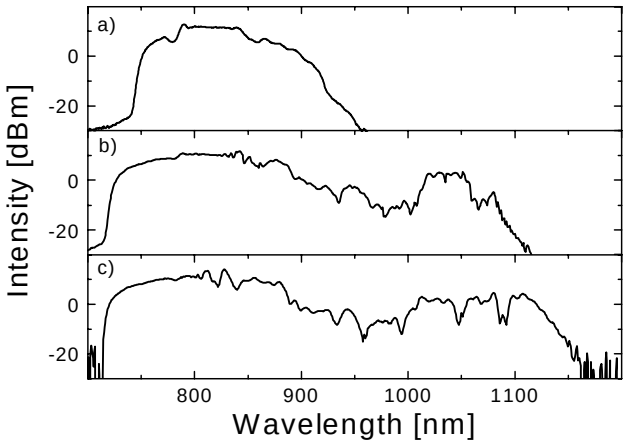

Fig. 16. Supercontinuum generated in 1 m of the round-core MF for different pulse widths. a) 300 fs, b) 200 fs, and c) 130 fs. λ_p =810 nm, P_{av}=100 mW.

#1605 - $15.00 US Received August 21, 2002; Revised September 25, 2002

Finally, as for the case of pumping on the anomalous side, we have simulated the spectrogram of the continuum formed in the 1 m long MF for λ_p=860 nm. The results presented in the animation in Fig. 17 clearly show the sequence of events described above. In particular, the SPM-induced broadening is evident as well as the formation of solitons and their subsequent wavelength shift due to Raman scattering as the continuum expands beyond the ZDW. The radiated wave corresponding to the Raman soliton with the longest wavelength is also observed.

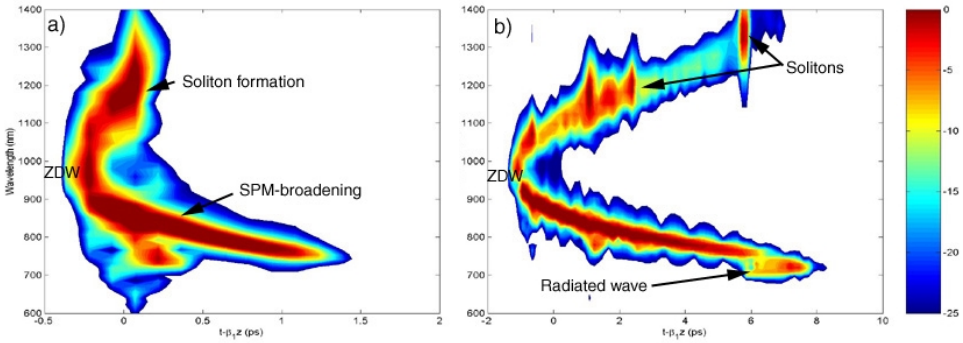

Fig. 17. Simulation of the spectrogram after a) 20 cm and b) 1 m of propagation along the round-core MF. P_{av}=120 mW, λ_p=860 nm, T_{FWHM}=130 fs. The normalized intensity is plotted in a logarithmic scale. The animation represents the formation of the continuum as the pulses propagate along the fiber, each frame corresponding to a step of 1 cm of propagation.

4. Conclusion

We have shown experimentally and numerically that the mechanisms leading to the formation of supercontinuum in microstructured fibers critically depend on the pump wavelength. We have explained in detail the formation of the continuum when the pump is located either in the anomalous or in the normal dispersion region of the fiber. In particular, we have found that Raman scattering plays a decisive role in the formation of the continuum and that the width of the continuum is governed by the group-delay profile of the fiber. We find experimentally that in the case of anomalous pumping, the nonlinear processes involved allow for the generation of supercontinuum when the pump wavelength is detuned by as much as 200 nm from the zero-dispersion wavelength. Pumping in the normal dispersion region of the fiber leads to supercontinuum formation through self-phase modulation and four-wave mixing. If the pump pulse is energetic enough and the spectrum extends to the anomalous side, Raman shifted solitons carry the spectrum further into the infrared.

Acknowledgments

We thank the Academy of Finland and the national graduate school GETA for funding the research and acknowledge the generosity of NKT Research and Innovation.

#1605 - $15.00 US Received August 21, 2002; Revised September 25, 2002